Membrane-Initiated Ca^{2+} Signals Are Reshaped during Propagation to Subcellular Regions

Werner J. H. Koopman,* Wim J. J. M. Scheenen,* Rachel J. Errington,†‡ Peter H. G. M. Willems,†
René J. M. Bindels,‡ Eric W. Roubos,* and Bruce G. Jenks*
Departments of *Cellular Animal Physiology, †Biochemistry, and ‡Cell Physiology, University of Nijmegen, Nijmegen, The Netherlands

ABSTRACT An important aspect of Ca^{2+} signaling is the ability of cells to generate intracellular Ca^{2+} waves. In this study we have analyzed the cellular and subcellular kinetics of Ca^{2+} waves in a neuroendocrine transducer cell, the melanotrope of *Xenopus laevis*, using the ratiometric Ca^{2+} probe indo-1 and video-rate UV confocal laser-scanning microscopy. The purpose of the present study was to investigate how local Ca^{2+} changes contribute to a global Ca^{2+} signal; subsequently we quantified how a Ca^{2+} wave is kinetically reshaped as it is propagated through the cell. The combined kinetics of all subcellular Ca^{2+} signals determined the shape of the total cellular Ca^{2+} signal, but each subcellular contribution to the cellular signal was not constant in time. Near the plasma membrane, $[Ca^{2+}]_i$ increased and decreased rapidly, processes that can be described by a linear and exponential function, respectively. In more central parts of the cell slower kinetics were observed that were best described by a Hill equation. This reshaping of the Ca^{2+} wave was modeled with an equation derived from a low-pass RC filter. We propose that the differences in spatial kinetics of the Ca^{2+} signal serves as a mechanism by which the same cellular Ca^{2+} signal carries different regulatory information to different subcellular regions of the cell, thus evoking differential cellular responses.

INTRODUCTION

Changes in cytosolic calcium levels ($[Ca^{2+}]_i$) serve as regulatory signals for a wide variety of cellular and subcellular functions (Bito et al., 1996; Burgoyne and Morgan, 1998; Deisseroth et al., 1998; Dolmetsch et al., 1998; Li et al., 1998; Petersen et al., 1999; Chin and Means, 2000). Each change in $[Ca^{2+}]_i$ is the result of an imbalance between calcium influx (from the extracellular medium and/or intracellular stores) and calcium removal (extrusion or sequestration). Modulation of the spatial arrangement of these influx and removal mechanisms could result in a Ca^{2+} signal with distinct differences in local kinetics. Although there is substantial insight into the mechanisms underlying subcellular signaling (Thorn et al., 1993, 1996; Bootman and Berridge, 1995; Lopez-Lopez et al., 1995; Bootman et al., 1997; Sham, 1997; Tse et al., 1997; Finch and Augustine, 1998; Petersen et al., 1999), little is known about how these changes are reflected in the global cellular Ca^{2+} signal.

The decoding of a Ca^{2+} signal into a cellular response is a complex process because it can occur at diverse subcellular levels. For instance, it has been established that exocytosis requires a high $[Ca^{2+}]$ (up to several hundreds of μM) for a short duration (μs–ms; Thomas et al., 1993; Chow et al., 1994; Burgoyne and Morgan, 1998), whereas activation of gene expression depends on more prolonged Ca^{2+} rises (s-min) (Bito et al., 1996; Dolmetsch et al., 1998; Li et al., 1998). This raises the question as to how a global cytosolic Ca^{2+} elevation can generate different subcellular Ca^{2+} responses.

We hypothesize that local Ca^{2+} changes contribute with different temporal kinetics to a global Ca^{2+} signal. One way this could occur is via intracellular Ca^{2+} waves whereby the Ca^{2+} signal changes its local kinetics as the wave travels through the cell. The aim of the present study was to investigate this hypothesis in studies of Ca^{2+} signaling in a neuroendocrine cell, the pituitary melanotrope of the amphibian *Xenopus laevis*. In its active state, the melanotrope cell displays spontaneous Ca^{2+} oscillations that are initiated by a membrane oscillator mechanism (Scheenen et al., 1994a; Koopman et al., 1997; Lieste et al., 1998). The rising phase of an oscillation is cumulatively built up by several discrete increases, the so-called "Ca^{2+} steps" (Scheenen et al., 1996; Koopman et al., 1997). Each step is associated with a short depolarization of the plasma membrane (Lieste et al., 1998) and is carried as a Ca^{2+} wave through the cytoplasm and into the nucleus. The oscillations are not only important in evoking the secretion of α-melanophore-stimulating hormone (α-MSH) from the melanotrope (Douglas and Shibuya, 1993; Shibuya and Douglas, 1993; Scheenen et al., 1994b, c), but also appear to be involved in the control of expression of the proopiomelanocortin (POMC) gene, which encodes the precursor protein for α-MSH (Dotman et al., 1997). Both secretion and gene expression in the melanotrope are under extracellular control through a variety of stimulatory and inhibitory neurotransmitters, the action of

Received for publication 19 October 2000 and in final form 16 April 2001.

Address reprint requests to Wim Scheenen, Dept. of Cellular Animal Physiology, Toernooiveld 1, University of Nijmegen, 6525 ED Nijmegen, The Netherlands. Tel.: +31-(0)24-3653335; Fax: +31-(0)24-3652714; E-mail: scheenen@sci.kun.nl.

W. J. H. Koopman's present address is Microscopical Imaging Center, University of Nijmegen, P.O. Box 9101, NL-6500 HB, Nijmegen, The Netherlands.

R. J. Errington's present address is Depts. of Cell Physiology and Medical Biochemistry, University of Wales College of Medicine, Heath Park, Cardiff CF4 4XN, UK.

0006-3495/01/07/57/09 $2.00

which, during signal integration, is to converge on the Ca^{2+} signaling machinery on the plasma membrane (Shibuya and Douglas, 1993; Scheenen et al., 1994a). Knowledge about how a cellular Ca^{2+} signal generated by a plasma membrane oscillator is reshaped in different subcellular regions will help in our understanding of signal integration, particularly the regulation of processes in diverse subcellular compartments. In this study we image $[Ca^{2+}]_i$ using the fluorescent calcium indicator indo-1 and high-speed UV confocal laser scanning microscopy (CLSM). We show that both the shape and kinetics of the Ca^{2+} signal are altered as it traverses the cell. These changes can be described mathematically by a model derived from an electronic low-pass filter.

MATERIALS AND METHODS

Materials

Indo-1/AM and Pluronic F127 were purchased from Molecular Probes Inc. (Leiden, The Netherlands) and dissolved in DMSO (2 μg/μl) to prepare stocks. Leibovitz's L15 medium, kanamycin, antibiotic/antimyotic, fetal calf serum, and trypsin were from Gibco (Life Technologies, Rockville, MD). Ultral-HEPES was from Calbiochem (La Jolla, CA). All other reagents were from Sigma (St. Louis, MO).

Cell preparation

Young-adult *Xenopus laevis*, taken from laboratory stock and kept under standardized conditions as previously described (Lieste et al., 1998), were anaesthetized in a solution containing 0.1g/l MS-222 (3-aminobenzoic acid ethyl ester) and 1.5 g/l $NaHCO_3$. Blood cells were removed before dissection by perfusion with *Xenopus* Ringer's solution (112 mM NaCl, 2 mM KCl, 2 mM $CaCl_2$, 2 mg/ml D-glucose, 1 μg/ml L-ascorbic acid, and 15 mM Ultral-HEPES; pH 7.4) containing MS-222 (0.1 g/l). Neurointermediate pituitary lobes were microdissected and incubated for 45 min in *Xenopus* Ringer's solution without $CaCl_2$ and containing 2.5 mg/ml trypsin. After gentle trituration through a narrow Pasteur's pipette, *Xenopus laevis* Leibovitz's L15 medium (XLL15, adjusted for *Xenopus* blood osmolarity and consisting of 67% (v/v) Leibovitz's L15 medium, 31% Milli-Q, 1% (v/v) kanamycin solution, 1% (v/v) antibiotic/antimyotic solution, 2 mM $CaCl_2$, and 10 mM D-glucose) with 10% (v/v) fetal calf serum were added to stop trypsin action, and the pars nervosa was removed by filtration. After centrifugation (10 min at 50 $\times$ *g*) the resulting pellet of melanotrope cells was resuspended in a small volume (50 μl/coverslip) of XLL15 medium and then put in the middle of 24-mm glass coverslips coated with high MW (>300 kDa) poly-L-lysine at a density of ~10,000 cells/slip. After the cells were allowed to attach for 60 min, 2 ml of XLL15 medium containing 10% (v/v) fetal calf serum was added. Before use, the cells were cultured for 3 days at 22°C in a humidified atmosphere.

Ratiometric Ca^{2+} measurements with indo-1

Coverslips were placed in a Leiden chamber (Ince et al., 1985) and the cells were loaded with indo-1/AM for 25 min after exchanging the XLL15 culture medium with a loading solution that consisted of *Xenopus* Ringer's solution containing 5 μM indo-1/AM and 0.025% (w/v) Pluronic F127. Then, cells were washed twice with *Xenopus* Ringer's solution and incubated another 15 min. Subsequently, the Leiden chamber was placed on a NIKON diaphot inverted microscope (Nikon, Tokyo, Japan) attached to an OZ CLSM (Noran Instruments, Middleton, WI). Excitation of indo-1 (at 351 nm) was provided by a high-power argon-ion laser (Coherent Enterprise, Santa Clara, CA). The estimated laser intensity at the back of the objective lens was 28 μW. Indo-1 fluorescence emission was monitored at 405 and 485 nm after separation with a 455 nm DCLP dichroic mirror. All experiments were done using a NIKON 40$\times$ water-immersion, 1.2 NA fluor objective lens. Confocality was achieved by using a slit-width of 100 μm. The user-controlled setup for hardware and acquisition was controlled by Intervision software (Version 1.5, Noran Instruments) running under IRIX 6.2 on an Indy workstation (Silicon Graphics Inc., Mountain View, CA). Full-frame images (512 $\times$ 480 pixels) were collected at 30 Hz and a pixel dwell time of 100 ns, or in band scanning mode (512 $\times$ 120 pixels) at 120 Hz. In the band scanning mode the signal-to-noise ratio was improved by applying a running average of two frames, thereby effectively reducing the sampling rate to 60 Hz.

A frame-store of 75 Mb was used, enabling 6 s (at 30 Hz) or 3 s (at 60 Hz) of continuous recording time. Pairs of fluorescence intensities were saved over time in SGI-movie format ready for off-line analysis. The (x, y) pixel dimensions were calibrated by using a microscope graticule in transmission or reflection mode. The length in pixels of the largest number of divisions that fitted inside the field of view was determined. Pixel size (in μm) was then calculated as the total length of the graticule (in μm) divided by the number of pixels. The optical section thickness was estimated with a test sample under the experimental conditions used. The axial intensity profile through a simple planar object (much thinner than the axial resolution) gives the plane response function (PRF) from which the section thickness is derived (Fricker et al., 1998) using the frame width at half-maximal height (FWHM; Cogswell and Larkin, 1995). Optical sections (x, y) were collected at 0.2 μm steps through the first coverglass/mirror interface. The image stack (x, y, z) was resampled to extract a single cut-plane image (x, z) through this interface. Subsequently, an intensity profile along the z axis was obtained and used for further analysis.

Spatial and temporal calibration of the setup

To evaluate the stability of image sampling, average sampling intervals were calculated to be 33.0 $\pm$ 0.0011 ms (SEM, n = 7013 intervals) at 30 images/s and 16.5 ms $\pm$ 0.0024 ms (SEM, n = 3000 intervals) at 60 images/s, accurately corresponding to the user setup. System performance in the axial (z) direction was evaluated by plotting vertical response profiles obtained at different slit widths (Fig. 1 *A*). When no slit was used, confocal section thickness was 10.5 μm. By using a 100-μm or 15-μm slit the section thickness was reduced to 2.8 μm and 1.2 μm, respectively. System performance tests demonstrated that small misalignments of the slit (three units) severely compromised axial (z) resolution (Fig. 1 *B*). Given the diameter of melanotropes from black-adapted *Xenopus* (15–20 μm) and the limitations imposed by the signal-to-noise ratio upon the ability to measure "local" signals, an optimally aligned 100 μm slit was applied in all recordings.

Data analysis

Ratio images (F405/F485) were calculated using the Intervision 2D software package (Noran Instruments). Visualization tools from the Intervision 3D software module were used to obtain cut-plane, resampled line data displays of ratio data. If needed, regions of interest (ROI) were drawn and numerical ratio values were stored in ASCII format. Additional analysis was carried out by using a dedicated data analysis program (Origin 6.0, Microcal, Northampton, MA), statistical package (Statistica 99, StatSoft Inc., Tulsa, OK) and mathematical software (Maple Vr5, Waterloo Maple Software, Waterloo, Ontario, Canada). Numerical data obtained from multiple recordings were expressed as average $\pm$ SD unless stated otherwise. Additional image analysis and visualization were performed with Image Pro 3.0 software (Media Cybernetics, Silver Spring, MD).

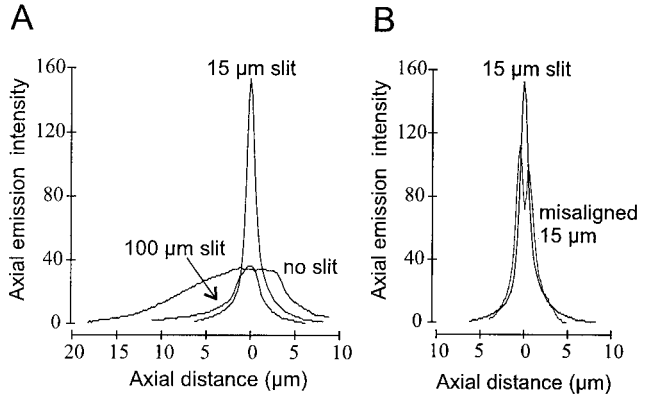

FIGURE 1 Spatial calibration of the confocal setup. (*A*) Intensity response profile in the *z*-direction of a flat mirror mounted above the objective at different widths of the confocal slit (see text for details). The frame width at half-maximal height (FWHM) was used as a measure for optical section thickness. The standard slit width used (100 μm) corresponds to a section thickness of 2.85 μm. (*B*) Degradation of image intensity by misalignment of the slit. Note the increased FWHM leading to a suboptimal sectioning thickness.

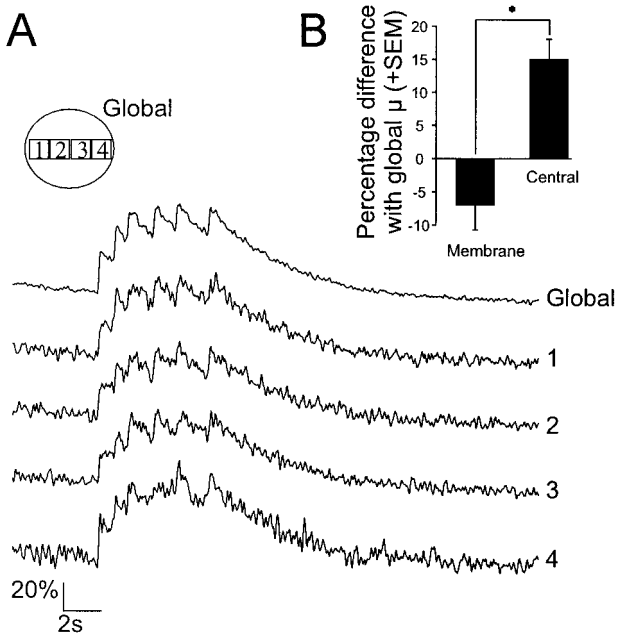

FIGURE 2 Subcellular kinetics of Ca^{2+} oscillations in melanotropes. (*A*) Ca^{2+} oscillations (one of which is shown) were recorded at 30 Hz from several rectangular subcellular ROIs and the total cell (see *inset*, marked 1 to 4 and Global). Six discrete steps were observed for each region. The Ca^{2+} decline at the end of the oscillation was fitted adequately by a monoexponential function. (*B*) The difference in the value of μ near the membrane and in central regions relative to that from the "global" signal, which was set at 100%. Central regions displayed a higher average μ than membrane regions ($p < 0.05$), indicative of a slower Ca^{2+} removal rate.

RESULTS

Spatiotemporal Ca^{2+} kinetics of oscillation decline phases

We first evaluated spatial differences in Ca^{2+} kinetics during the decline phase of the Ca^{2+} oscillations using a sampling speed of 30 Hz. In *Xenopus* melanotropes this decline phase is slow and can take up to 30 s (Lieste et al., 1998). Four ROIs were chosen spanning the total cell diameter (Fig. 2 *A*), each covering an area between 12 and 15 μm^2. For comparison, the indo-1 signal for the complete cellular volume within the confocal plane was also recorded (marked "Global"). Although the noise present in the recording did not allow a detailed kinetic analysis of the rising phase of the oscillation, six discrete Ca^{2+} steps could be clearly distinguished. At the end of the series of steps the indo-1 signal returned smoothly to basal level in a monoexponential fashion ($y = y_0 + Ae^{-t/\mu}$). We used the decay time constant μ of the exponential, being inversely proportional to the Ca^{2+} removal rate, to quantify spatial differences in Ca^{2+} removal kinetics. Comparison of the Ca^{2+} removal kinetics between ROIs 1 ($\mu = 4.25$) and 4 ($\mu = 4.24$) near the plasma membrane and more central ROIs 2 ($\mu = 4.60$) and 3 ($\mu = 4.76$) showed that membrane regions displayed a lower μ value than central regions, i.e., a faster Ca^{2+} removal rate. For visualization purposes, the decay rate of each region was expressed as the difference with the global decay rate, which was set at 100% (Fig. 2 *B*, $n = 11$ cells; $p < 0.05$).

Three-dimensional representation of (*x*, *y*, *t*) data

For further analysis of the rising phase of the Ca^{2+} oscillation, a method was required to quickly visualize large indo-1 data sets with a sufficiently high signal-to-noise ratio. Therefore, 150 indo-1 ratio images, obtained with 30 Hz sampling speed, were stacked in a 3D framework (Fig. 3). Before ratioing, each single wavelength image pair was background-corrected and spatially filtered with a 3×3 median filter. A false color lookup table was used for color-coding the gray values. By reslicing of the (x, y, t) dataset, a Ca^{2+} change could be investigated at any desired x, y coordinate as a function of time. For the cell shown, a reslicing was performed at the locations shown in Fig. 3 *A* (*red lines*), resulting in two cellular cross sections of the data: an Xt stack (Fig. 3 *B*) and a Yt stack (Fig. 3 *C*). In this typical recording the melanotrope cell displays several discrete Ca^{2+} changes ("steps"), and each of these steps clearly showed up as a Ca^{2+} wave in the Xt and Yt scan (Fig. 3, *B* and *C*). The calculated wave speeds were between 30 and 70 μm/s ($n = 6$), in agreement with earlier line-scan studies performed with Fura Red (Scheenen et al., 1996; Koopman et al., 1997) and Oregon-green 1 (Koopman et al., 1999). Throughout this study we used the 3D visualization method for rapid screening and selection of appropriate data sets for analysis.

Given the fact that in *Xenopus* melanotropes each Ca^{2+} wave moves concentrically inward from the plasma membrane in the confocal plane (Koopman et al., 1997

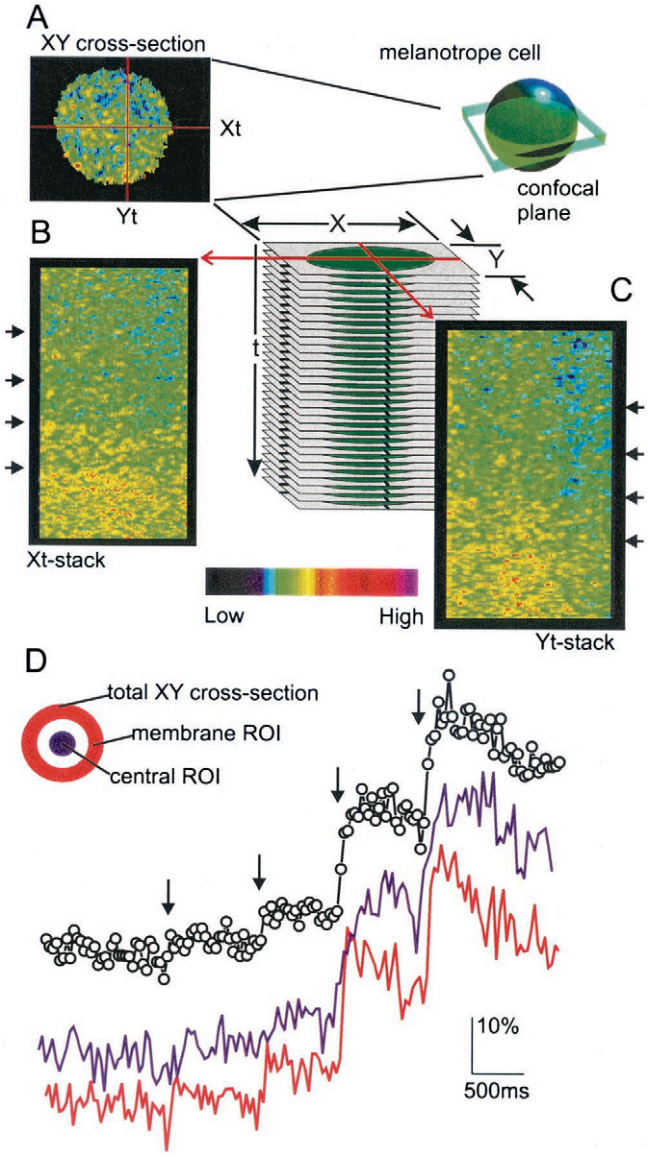

FIGURE 3 Rapid visualization and screening of large (x, y, t) data sets. (*A*) Top view of a single confocal XY cross section obtained at the indicated confocal plane. A linear lookup table was used for false color visualization. By vertically stacking 150 successively recorded indo-1 ratio images (at 30 Hz) from top to bottom in a 3D framework (3D-stack), a (x, y, t) data set is obtained. The (x, y, t) data set was resliced perpendicularly to the plane of the paper, across the red lines marked Xt and Yt (schematically shown in the diagram and in *A*). (*B*) Xt image obtained by reslicing via line Xt in *A*. The image shows four discrete Ca^{2+} rises visible as increases in signal intensity (*arrows*). (*C*) Image obtained by reslicing via line Yt, also showing four discrete Ca^{2+} rises (*arrows*). (*D*) Comparison of the global Ca^{2+} signal (black line derived from the total cellular cross section in *A*), and two regions of interest (ROIs) located near the plasma membrane (*red line*) and in the center of the cell (*blue line*). Four discrete Ca^{2+} rises can be distinguished. The observed Ca^{2+} kinetics in the selected regions differ considerably.

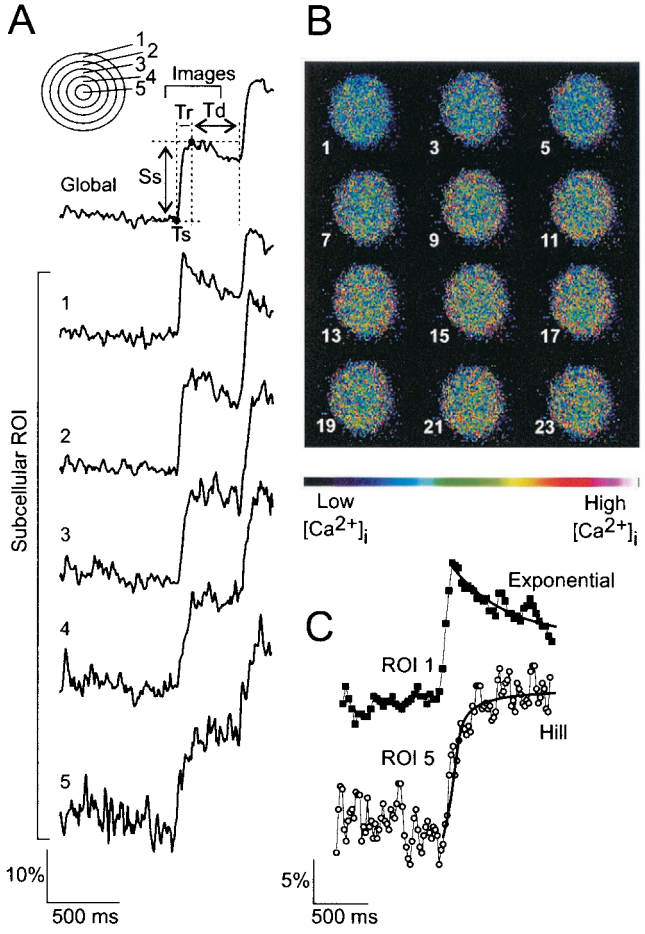

FIGURE 4 Kinetic reshaping of propagating Ca^{2+} waves. (*A*) Reshaping of Ca^{2+} steps observed upon transition of the Ca^{2+} wave from ROI 1 to the central ROI 5 (see *inset* for ROI definition). The global cellular Ca^{2+} signal is shown on top and the time span at which the images in (*B*) were taken is indicated. Spatiotemporal differences in kinetics were quantified using several parameters (marked by T_r, T_d, S_s, and T_s), which are described in the results and listed in Table 1. (*B*) Indo-1 ratio images recorded at 30 Hz showing the first Ca^{2+} step in (*A*). The image set was recorded at 60 Hz, but for display each second image has been omitted from the figure. A linear lookup table was used to color-code indo-1 ratios. Cell radius was 11.75 μm with an optical section thickness of 2.85 μm. The Ca^{2+} wave can be seen as a ring as it travels from the plasma membrane to the central part of the cell. (*C*) An enlargement of the first step for ROI 1 (close to the plasma membrane) and the central ROI 5, showing that a monoexponential equation fits Ca^{2+} dynamics of ROI 1, whereas a Hill equation properly fits the Ca^{2+} dynamics of region ROI 5.

and Fig. 4 *A* and *B*), we used circular ROIs to extract numerical data from the indo-1 images (*inset* in Fig. 3 *D*). This approach led to a considerable noise reduction (compare plasma membrane and central traces in Fig. 3 with Fig. 2 *A*), and indicated that the Ca^{2+} kinetics between subcellular regions might be kinetically different from each other, with the decay more rapid in the membrane ROI (Fig. 3 *D*). However, the temporal resolution in this experiment was not sufficiently high to quantify these differences. Therefore, in the next set of experiments the local differences in the Ca^{2+} dynamics were examined at a higher sampling speed.

Kinetics of a Ca^{2+} wave

To assess the spatiotemporal nature of the heterogeneous Ca^{2+} signaling during the rising phase of an oscillation, images were sampled at 60 Hz. The effective signal-to-noise ratio was optimized during analysis by using ring-shaped ROIs that successively decreased in size (Fig. 4 *A*). With decreasing surface area of the ROIs, the noise present in the signal increased monoexponentially ($\mu = 10 \pm 3$, $\chi^2 = 5 \cdot 10^{-5}$). However, this increase in noise did not hamper our analysis.

We calculated the area of the ROIs by considering the "Global" ROI and ROI 5 as a circle and the other ROIs as rings. Fig. 4 *B* shows indo-1 ratio images taken during the rising phase of the first step (marked in the global trace of Fig. 4 *A* with "images"). Every second image was omitted and a false color look-up table was added. This figure demonstrates that the Ca^{2+} wave associated with the step moves in a ring-like fashion from the plasma membrane to the central part of the cell, justifying the use of ring-like ROIs. The following parameters were quantified for each ROI ($n = 9$, Fig. 4 *A* and Table 1): 1) T_s, the starting time of a step, estimated using the CUSUM method (Koopman et al., 1996, 1997); 2) T_r, the rise time of a step; 3) T_d, the duration of the Ca^{2+} decline between two steps; 4) S_s, the size of a step; 5) V_r, the rise speed of a step (given by S_s/T_r); and 6) V_d, the decline speed between steps approximated with a linear model (Lieste et al., 1998).

For the first step, progressing from the plasma membrane (ROI 1) to the center of the cell (ROI 5) an increase in T_s, T_r, and S_s, but a reduction in T_d, V_r, and V_d, was observed (Table 1). Similar results were obtained for the second step and steps in other cells. In ROI 2 a periodic component of ~10 Hz was observed which, however, was not present in the other ROIs, nor in other cells measured. Because this 10 Hz pattern in ROI 2 is not seen in subsequent ROIs, it is probably noise-related and most likely does not reflect actual changes in $[Ca^{2+}]_i$. To demonstrate spatial differences in Ca^{2+} kinetics more clearly, ROI 1 was plotted next to ROI 5 (Fig. 4 *C*). As mentioned before, in ROI 1, T_r and V_d were faster than in ROI 5, and the S_s of the step in ROI 5 were larger than in ROI 1 (Table 1). The decline in ROI 1 was described well by a single exponential model. A Ca^{2+} removal rate (μ) of $0.294 \pm 6.5 \cdot 10^{-3}$ ($\chi^2 = 9 \cdot 10^{-5}$) was found. In the central region no decline was observed and a Hill equation was appropriate to fit the $[Ca^{2+}]_i$ kinetics (with $V_{max} = 1.168 \pm 3.8 \cdot 10^{-3}$, $k = 1.45 \pm 0.023$, $n = 15.33 \pm 1.83$, $\chi^2 = 3.6 \cdot 10^{-4}$).

Contribution of intracellular regions to the global Ca^{2+} signal

To estimate the contribution of each intracellular region to the global Ca^{2+} signal during the occurrence of a Ca^{2+} step, the pre-normalized recordings obtained from the circular regions shown in Fig. 4 *A* were analyzed. The indo-1 ratio obtained from the total cellular ROI (Fig. 5 *A*) was used to define the starting time (T_s), the time to reach the peak (T_p), and the ending time (T_e) of the first step (*dotted vertical lines*). By definition, each indo-1 ratio time recording ($R(t)_n$) for a certain ROI n is given as a function of time by the integrated ratio ($R_i(t)_n$) divided by the area (A_n) of the ROI: $R(t)n = R_i(t)_n/A_n$. For each time point the relative contribution W (weight) of the ROI to the total indo-1 ratio can then be expressed as $W(t) = [R_i(t)_n/R_i(t)_t] \times 100\%$ (Fig. 5 *C*).

The sum of all $W(t)$ values before the Ca^{2+} step was 100% and increased to 114% after the step. This 14% increase was equal to the size of the global Ca^{2+} step (Fig. 4 *A*). All $W(t)$ values at T_e were different from those before the step occurred ($p < 0.001$; determined by comparing the average $W(t)$ value of 10 points at the beginning and at the end of the recording). The contribution $W(t)$ to the total Ca^{2+} rise by ROI 1 gradually decreased toward T_e, whereas $W(t)$ for the other intracellular regions increased (Fig. 5 *B*). During the rising phase of the step, ROI 1 and 2 showed a transiently increased contribution to the global indo-1 signal (Fig. 5 *C*), while at the same time ROI 3 and 4 showed a decrease in $W(t)$. ROI 5 showed the same trend as ROI 3 and 4, but the profile was very noisy and therefore left out of the figure. The $W(t)$ traces shown are expressed as normalized

TABLE 1 Numerical kinetic data derived from Fig. 4

ROI	d_{mem} (μm)	*XY* Area (μm^2)	T_s (ms)	T_r (ms)	T_d (ms)	S_s (A.U.)	V_r (A.U./s)	V_d (A.U./s)
Global	n.a.	434 (100%)	n.a.	217	633	1.16	5.35	-0.049 ± 0.00049
1	2.45	162 (37%)	0	84	766	1.16	13.81	-0.067 ± 0.0067
2	4.93	125 (29%)	16.5	217	617	1.21	5.58	-0.099 ± 0.011
3	6.98	75 (17%)	66	326	533	1.20	3.68	-0.038 ± 0.020
4	8.92	46 (11%)	116	433	400	1.20	2.77	-0.003 ± 0.010
5	11.75	20 (5%)	182	517	420	1.28	2.48	0.015 ± 0.017

Numerical data for the ROIs shown in Fig. 4, obtained after a spatiotemporal calibration of the confocal setup with an optical section thickness of 2.85 μm. For each region used in Fig. 4 an appropriate calculation was carried out to estimate the area of each ROI (*XY* area). Abbreviations used: ROI, region of interest; d_{mem}, distance of the inner ring of the ROI from plasma membrane; *XY* area, confocal surface area of the ROI; T_s, time at which the Ca^{2+} rise starts relative to ROI 1; T_r, time needed for a step to rise, T_d, time for Ca^{2+} removal between steps; S_s, size of step ($=R_{max}/R_{min}$); V_r, linear rise-speed of step calculated from (S_s/T_r); V_d, decline speed ($\pm$SD) of step estimated from a linear fit to the ratio values.

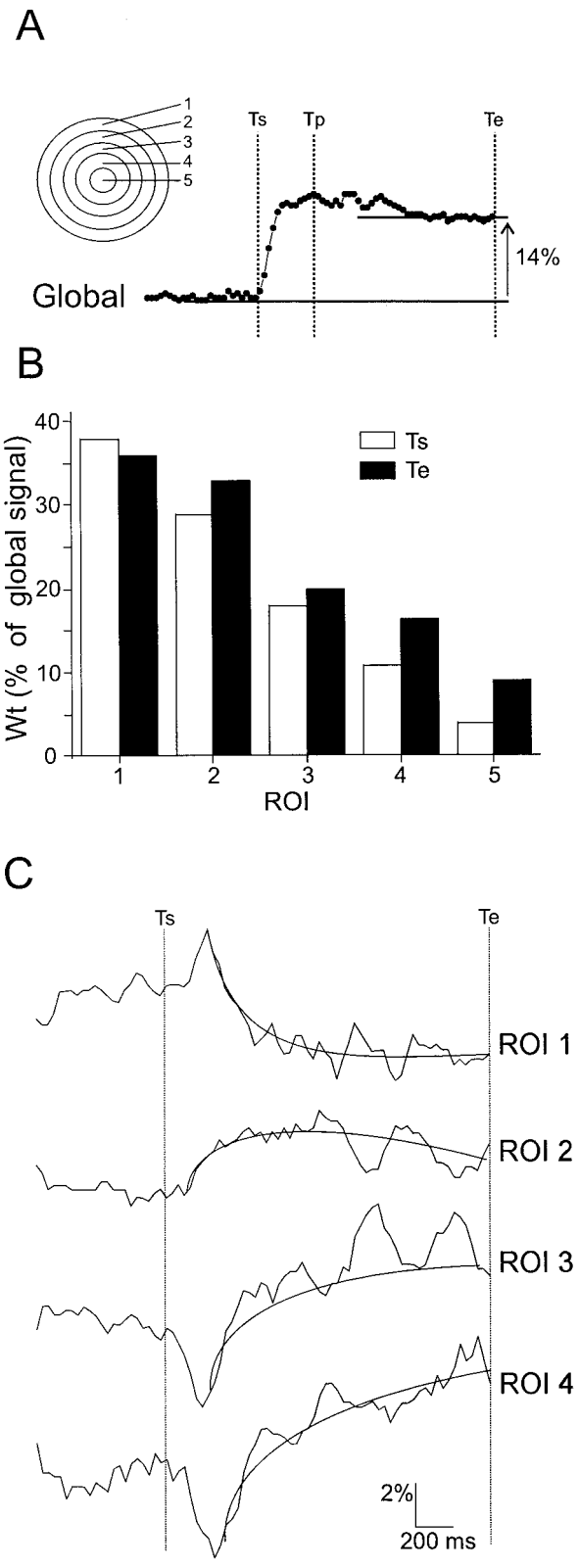

FIGURE 5 Contribution of local Ca^{2+} changes to the global Ca^{2+} signal. (*A*) Average global Ca^{2+} signal, with marked starting time (T_s), peak time (T_p), and ending time (T_e) of the Ca^{2+} step. The *inset* shows the location of the ROIs. (*B*) Percent contribution (Wt) of each ROI to the global Ca^{2+} signal before (T_s; *open bars*) and after (T_e; *closed bars*) occurrence of a step (see Results for calculation details). (*C*) Normalized traces showing the contribution (Wn) of various regions to the total Ca^{2+} signal as a function of time before, during, and after a Ca^{2+} step. The general trend is depicted by the curves (the trace for ROI 5 was noisy and therefore not included in figure).

percent of the global indo-1 ratio signal. In general, during the rising phase of the Ca^{2+} oscillations, the contribution to the total indo-1 signal increased for central regions and decreased for regions near the plasma membrane (curves drawn in Fig. 5 *C*).

Modeling of Ca^{2+} kinetics with an RC filter

The attenuation of the kinetics of the Ca^{2+} step (and its associated wave) upon transition from the plasma membrane to the center of the cell strongly resembles the behavior of a low-pass RC filter. Therefore, we used such an RC filter in a mathematical model to describe the reshaping of the calcium step during this transition (Fig. 6 *A*). An electronic RC circuit (Fig. 6 *A*, "RC circuit") consists of a resistor placed in parallel to a capacitor and transforms a rapidly changing input voltage ($V_i(t)$) into a smoothed output voltage ($V_o(t)$) (Brooks, 1985). By increasing the RC value (given by the product of R and C) of the circuit, the amount by which high frequencies are filtered out of $V_i(t)$ can be increased. An electronic RC filter can be mathematically described by:

$$V_o(t) = V_i(t) - RC\frac{d[V_o(t)]}{dt}. \quad (1)$$

For finite Δt, this differential equation transforms into:

$$V_o(t) = V_i(t) - RC\frac{V_o(t) - V_o(t + \Delta t)}{\Delta t}. \quad (2)$$

Equation 2 was rewritten for computer implementation and adapted for calcium signaling by substitution of $V_i(t)$ by $Ca^{2+}(t)_m$ (the Ca^{2+} trace recorded at the membrane) and $V_o(t)$ by $Ca^{2+}(t)_c$ (the calcium trace calculated at the center of the cell). This gives:

$$Ca^{2+}(t)_c = x[Ca^{2+}(t)_m] + (1 - x)[Ca^{2+}(t - \Delta t)_c]. \quad (3)$$

in which $x = \Delta t/(RC + \Delta t)$ and Δt = sampling interval. This equation was used to predict the Ca^{2+} signal in the center of the cell from an experimentally obtained membrane Ca^{2+} signal. The RC filter in this form failed to correctly predict $Ca^{2+}(t)_c$ from a given $Ca^{2+}(t)_m$ (four of nine cells) because the amplitude of $Ca^{2+}(t)_c$ was underestimated (data not shown). Therefore, we introduced an amplification factor y, thereby transforming Eq. 3 into:

$$Ca^{2+}(t)_c = x[Ca^{2+}(t)_m] + (1 - x)[Ca^{2+}(t - \Delta t)_c]^y. \quad (4)$$

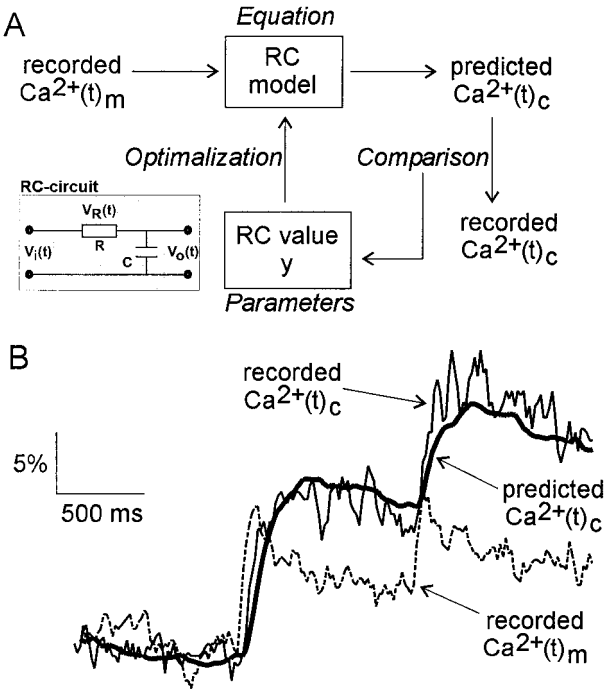

FIGURE 6 An RC circuit describes reshaping of Ca^{2+}. (*A*) The RC circuit (*inset*) and the calculation scheme used for estimation of RC value and amplification factor *y*, which are parameters of the RC model. The recorded Ca^{2+} trace at the plasma membrane ($Ca^{2+}(t)_m$) was used to predict the Ca^{2+} signal in the center of the cell ($Ca^{2+}(t)_c$). The numerical values of *RC* and *y* were iteratively optimized by comparing the $Ca^{2+}(t)_c$ predicted by the model with the experimental $Ca^{2+}(t)_c$. (*B*) Comparison of a Ca^{2+} trace recorded at the membrane (*dotted line*), predicted by the RC model (*thick line*), and recorded in the center of the cell (*thin line*). The correlation between the predicted and recorded trace was 0.94 (with an RC value of 247 and a *y* value of 2.3).

When no amplification occurred, *y* was set to 1. For five cells the $Ca^{2+}(t)_c$ was higher than the $Ca^{2+}(t)_m$, implying that $y > 1$. For the cell shown, *y* was empirically set to 2.3, thereby increasing the predictive quality of the RC model. To further improve the performance of the model we estimated the optimal RC value (RC_{opt}), by using the Pearson's correlation coefficient (r; $r \in [0, 1]$) between the generated output and experimental data. RC_{opt} was estimated by calculation of r as $f(RC)$ and fitting this curve with a fifth-order polynomial function. By numerically estimating the extreme of this polynome (i.e., where r is maximal), an RC_{opt} of 247 was found for the cell shown. In Fig. 6 *B* the experimental $Ca^{2+}(t)_m$ is shown as a dotted line, the $Ca^{2+}(t)_c$ predicted by the model (Eq. 4) is indicated as a thick line, and the actual recorded $Ca^{2+}(t)_c$ is shown as a thin line. Combined with a *y*-value of 2.3 for the trace shown, the recorded $Ca^{2+}(t)_c$ was predicted with $r = 0.94$. In general, we were able to predict Ca^{2+} changes with an accuracy of $0.01 < p < 0.05$ ($n = 9$) (i.e., for the cells analyzed, the fit of the model was between 99.9% and 99% accurate, as calculated from the correlation between experimental traces and the model prediction).

DISCUSSION

Earlier line-scanning studies have shown that in *Xenopus* melanotropes Ca^{2+} waves are initiated at the plasma membrane and move concentrically inward (Scheenen et al., 1996; Koopman et al., 1997). In addition, it was found that the kinetics of the Ca^{2+} wave are different in different places in the cell. Because these studies were performed with non-ratiometric Ca^{2+} probes, they might suffer from artifacts such as dye compartmentalization, leakage, and photobleaching (Scheenen et al., 1996). Furthermore, spatial information had to be sacrificed to improve temporal resolution. Given these limitations, no detailed analysis of the kinetics of the Ca^{2+} signal in different parts of the cell could be performed. In the present study we examined whether global Ca^{2+} changes carried by a Ca^{2+} wave are kinetically reshaped in different subcellular areas, thereby giving rise to different Ca^{2+} signals. Therefore, we analyzed the global cellular and the subcellular kinetics of Ca^{2+} waves during Ca^{2+} oscillations in *Xenopus* melanotropes, using the ratiometric Ca^{2+} probe indo-1 and video-rate UV confocal laser scanning microscopy. Given the fast kinetics of the Ca^{2+} wave, cells were imaged at rates of 30 and 60 Hz. The data sets obtained were rapidly screened by visualizing them in three dimensions and then resliced in any required direction. In this way, cut-plane images were obtained that resembled "classical" line-scan recordings in the cut plane. A major advantage of this method is that it allows quick evaluation of the data with no a priori knowledge about the direction of wave movement.

By using the above procedure we confirm earlier studies which suggested that in melanotrope cells of *Xenopus laevis* the Ca^{2+} signals move as waves from the plasma membrane to the center of the cell. This concentrical propagation pattern, in combination with the spherical morphology of the cell, allowed us to maximize the area of each ROI by using ring-like regions. This was important to optimize signal-to-noise ratios. The wave speeds found were similar to those reported by Fura-Red (Scheenen et al., 1996; Koopman et al., 1997) and Oregon-Green I (Koopman et al., 1999). During oscillations, $[Ca^{2+}]_i$ increased most rapidly in the direct vicinity of the plasma membrane. In addition, Ca^{2+} was removed faster near the plasma membrane than in the center of the cell. The fast Ca^{2+} removal in close vicinity of the plasma membrane most likely reflects its extrusion into the extracellular space via plasma membrane Ca^{2+} ATPases or Ca^{2+} exchangers. Physiologically, this time course of rapid rise and decline in $[Ca^{2+}]_i$ near the plasma membrane might function as a way to optimally regulate exocytosis and endocytosis. In this respect it is noteworthy to mention that the total duration of a Ca^{2+} step, including decline time, of our studies (~1 s) falls within the reported time course of the granule fusion reaction in endocrine cells (between 0.02 and 10 s, Kasai, 1999).

At the end of each burst of Ca^{2+} steps both the Ca^{2+} level near the plasma membrane and in the center of the cell declined with monoexponential kinetics. This is in agreement with earlier findings obtained with whole-cell microfluorometry (Lieste et al., 1998). Because a single exponential function was adequate to describe the Ca^{2+} removal process, we suggest that Ca^{2+} removal occurs through a single, major pathway or several pathways with similar kinetics. In this study we demonstrated that the kinetics of the Ca^{2+} wave is altered during its travel to the cell interior. Therefore, a global Ca^{2+} signal is not necessarily kinetically similar to the signals in subcellular compartments of which it is constituted.

To estimate how subcellular Ca^{2+} changes contribute to the global Ca^{2+} signal we analyzed how the former changes contribute to the kinetics of the global Ca^{2+} change during individual Ca^{2+} steps. It was found that this contribution is not constant, but changes as a function of time. The membrane region makes the largest contribution early in a step, followed by progressively more important contributions of more centrally located regions of the cell later in the step. We show that the reshaping of the Ca^{2+} wave can be modeled by introducing an amplification factor into a standard low-pass (RC) filter. We have demonstrated earlier that wave propagation in *Xenopus* melanotrope cells involves a Ca^{2+}-induced Ca^{2+} release (CICR) mechanism (Koopman et al., 1999). The necessity of an amplification factor in the RC model could reflect action of such a CICR mechanism, as it would add additional Ca^{2+} to the wave during its propagation. On a molecular level, the RC filter could consist of a combination of CICR mechanisms, Ca^{2+} ATPases, or Ca^{2+}-binding proteins that are differentially expressed throughout the cell (Naraghi et al., 1998). We are currently investigating whether the mentioned CICR mechanisms indeed constitute the RC filter.

Interior regions and organelles, such as the nucleus, will be exposed to Ca^{2+} changes with distinct (slower) kinetics than those generated at the plasma membrane. Additionally, high-frequency signals like stochastic Ca^{2+} entry across the plasma membrane are effectively filtered out by the cytosolic RC filter, thereby preventing the induction of intracellular Ca^{2+} waves. The slower removal of Ca^{2+} from interior sites, in combination with the repetitive nature of the steps, may serve as a mechanism to activate effectors with a low affinity for Ca^{2+}. By tuning the RC value (i.e., its filtering strength), the cytosolic low-pass filter could thus provide a mechanism that enables differential activation of effector proteins in the interior of the cell, for example via calmodulin-mediated mechanisms (Chin and Means, 2000). In this way regulatory neurotransmitters, through action on membrane receptors, are capable of reliable signal transduction both near the plasma membrane and deep in the melanotrope cell.

We thank R. J. C. Engels for animal care.

This project was supported by NWO Equipment Grant 903-68-333.

REFERENCES

Berridge, M. J. 1997. The AM and FM of calcium signaling. *Nature.* 386:759–760.

Bito, H., K. Deisseroth, and R. W. Tsien. 1996. CREB phosphorylation and dephosphorylation: a Ca^{2+} and stimulus duration-dependent switch for hippocampal gene expression. *Cell.* 87:1203–1214.

Bootman, M. D., and M. J. Berridge. 1995. The elemental principles of calcium signaling. *Cell.* 83:675–768.

Bootman, M. D., M. J. Berridge, and P. Lipp. 1997. Cooking with calcium: the recipes for composing global signals from elementary events. *Cell.* 91:367–373.

Brooks, C. 1985. Microelectronics: Devices and Applications. National Education Corporation, USA.

Burgoyne, R. D., and A. Morgan. 1998. Calcium sensors in regulated exocytosis. *Cell Calcium.* 24:367–376.

Chin, D., and A. R. Means. 2000. Calmodulin: a prototypical calcium sensor. *Trends Cell Biol.* 10:322–328.

Chow, R. H., J. Klingauf, and E. Neher. 1994. Time course of Ca^{2+} concentration triggering exocytosis in neuroendocrine cells. *Proc. Natl. Acad. Sci. U.S.A.* 88:9883–9887.

Cogswell, C. J., and K. G. Larkin. 1995. The specimen illumination path and its effects on image quality. *In* Handbook of Biological Confocal Microscopy. J. B. Pawley, editor. Plenum Press, New York. 127–137.

Deisseroth, K., K. E. Heist, and R. W. Tsien. 1998. Translocation of calmodulin to the nucleus supports CREB phosphorylation in hippocampal neurons. *Nature.* 392:198–202.

Dolmetsch, R. E., K. Xu, and R. S. Lewis. 1998. Calcium oscillations increase the efficiency and specificity of gene expression. *Nature.* 392: 933–936.

Dotman, C. H., A. Maia, P. M. J. M. Cruijsen, B. G. Jenks, and E. W. Roubos. 1997. Differential action of secreto-inhibitors on proopiomelanocortin biosynthesis in the intermediate pituitary of *Xenopus laevis*. *Neuroendocrinology.* 66:106–113.

Douglas, W. W., and I. Shibuya. 1993. Calcium signals in melanotrophs and their relation to autonomous secretion and its modification by inhibitory and stimulatory ligands. *Ann. N.Y. Acad. Sci.* 680:229–245.

Finch, E. A., and G. J. Augustine. 1998. Local calcium signaling by inositol-1,4,5-trisphosphate in Purkinje cell dendrites. *Nature.* 396: 753–756.

Fricker, M., R. Errington, J. Wood, M. Tlalka, M. May, and N. White. 1998. Quantal confocal fluorescence measurements in living tissue. *In* Signal Transduction—Single Cell Techniques. B. Van Duijn and A.W-iltink, editors. Springer, New York.

Ince, C., J. T. Van Dissel, and M. C. Diesselhoff. 1985. A Teflon culture dish for high-magnification microscopy and measurements in single cells. *Pflügers Arch.* 403:240–244.

Kasai, H. 1999. Comparative biology of Ca^{2+}-dependent exocytosis: implications of kinetic diversity for secretory function. *Trends Neurosci.* 22:88–93.

Koopman, W. J. H., M. A. Hink, A. J. G. W. Visser, E. W. Roubos, and B. G. Jenks. 1999. Evidence that Ca^{2+} waves in *Xenopus* melanotropes depend on calcium-induced calcium release: a fluorescence correlation microscopy and line-scanning study. *Cell Calcium.* 26:59–67.

Koopman, W. J. H., B. G. Jenks, E. W. Roubos, and W. J. J. M. Scheenen. 1996. Retrieving spatiotemporal information from confocal data: a study using melanotrope cells of *Xenopus laevis*. *In* Fluorescence Microscopy and Fluorescent Probes. J. Slavik and K. Howell, editors. Plenum, New York.

Koopman, W. J. H., W. J. J. M. Scheenen, E. W. Roubos, and B. G. Jenks. 1997. Kinetics of calcium steps underlying calcium oscillations in melanotrope cells of *Xenopus laevis*. *Cell Calcium* 22:167–178.

Li, W., J. Llopis, M. Whitney, G. Zlokarnik, and R. Y. Tsien. 1998. Cell-permeant caged $InsP_3$ shows that Ca^{2+} spike frequency can optimize gene expression. *Nature.* 392:936–941.

Lieste, J. R., W. J. H. Koopman, V. C. J. Reynen, W. J. J. M. Scheenen, B. G. Jenks, and E. W. Roubos. 1998. Action currents generate stepwise

intracellular Ca^{2+} patterns in a neuroendocrine cell. *J. Biol. Chem.* 273:25686–25694.

Lopez-Lopez, J. R., P. S. Shacklock, C. W. Balke, and W. G. Wier. 1995. Local calcium transients triggered by single L-type calcium channel currents in cardiac cells. *Science.* 268:1042–1045.

Naraghi, M., T. H. Müller, and E. Neher. 1998. Two-dimensional determination of the cellular Ca^{2+} binding in bovine chromaffin cells. *Biophys. J.* 78:1635–1647.

Petersen, O. H., D. Burdakov, and A. V. Tepikin. 1999. Polarity in intracellular calcium signaling. *Bioessays.* 21:851–860.

Scheenen, W. J. J. M., H. P. de Koning, B. G. Jenks, H. Vaudry, and E. W. Roubos. 1994b. The secretion of α-MSH from *Xenopus* melanotropes involves calcium influx through ω-conotoxin-sensitive voltage-operated calcium channels. *J. Neuroendocrinol.* 4:457–464.

Scheenen, W. J. J. M., B. G. Jenks, E. W. Roubos, and P. H. G. M. Willems. 1994a. Spontaneous calcium oscillations in *Xenopus laevis* melanotrope cells are mediated by ω-conotoxin sensitive calcium channels. *Cell Calcium.* 15:36–44.

Scheenen, W. J. J. M., B. G. Jenks, R. J. A. M. Van Dinter, and E. W. Roubos. 1996. Spatial and temporal aspects of Ca^{2+}-oscillations in *Xenopus laevis* melanotrope cells. *Cell Calcium.* 19:219–227.

Scheenen, W. J. J. M., B. G. Jenks, P. H. G. M. Willems, and E. W. Roubos. 1994c. Action of stimulatory and inhibitory α-MSH secretagogues on spontaneous calcium oscillations in melanotrope cells of *Xenopus laevis*. *Eur. J. Physiol.* 427:244–251.

Sham, J. S. 1997. Ca^{2+}-release-induced inactivation of Ca^{2+}-current in rat ventricular myocytes: evidence for local Ca^{2+}-signaling. *J. Physiol. Lond.* 500:285–295.

Shibuya, I., and W. W. Douglas. 1993. Spontaneous cytosolic calcium pulsing detected in *Xenopus* melanotrophs: modulation by secretoinhibitory and stimulant ligands. *Endocrinology.* 132:2166–2175.

Thomas, P., J. G. Wong, and W. Almers. 1993. Millisecond studies of secretion in single rat pituitary cells stimulated by flash photolysis of caged Ca^{2+}. *EMBO J.* 12:303–306.

Thorn, P., A. M. Lawrie, P. M. Smith, D. V. Gallacher, and O. H. Petersen. 1993. Local and global cytosolic Ca^{2+}-oscillations in exocrine cells evoked by agonists and inositol trisphosphate. *Cell.* 74:661–668.

Thorn, P., R. Moreton, and M. J. Berridge. 1996. Multiple, coordinated Ca^{2+}-release events underlie the inositol trisphosphate-induced local Ca^{2+} spikes in mouse pancreatic acinar cells. *EMBO J.* 15:999–1003.

Tse, F. W., A. Tse, B. Hille, H. Horstmann, and W. Almers. 1997. Local Ca^{2+} release from internal stores controls exocytosis in pituitary gonadotrophs. *Neuron.* 18:121–132.